Signal enhancement and Patterson-search phasing for higher-spatial-resolution coherent X-ray diffraction imaging of biological objects

Coherent X-ray diffraction imaging (CXDI) is a lensless imaging technique for the structural analysis of non-crystalline samples typically with micron to submicron dimensions [1]. In CXDI experiments (Fig. 1), spatially coherent X-rays irradiate an isolated sample object, and the Fraunhofer diffraction pattern from the object is recorded on a detector. When the pattern is sampled at a spacing finer than the Nyquist interval (oversampling condition), phase information of the object can be directly recovered from the diffraction pattern with iterative phase retrieval (PR) algorithms. Thereby, we can obtain an electron density map of sample objects projected along the direction of the incident beam. The short wavelength and high penetration depth of X-rays allow visualization of the internal structures of whole objects that are too thick for analysis with electron microscopy with resolution beyond the limit of optical microscopy.

Biological samples are extremely sensitive to radiation, even at cryogenic temperatures, yet need to be imaged with significant doses of X-rays due to their small scattering cross section. X-ray free-electron laser (XFEL) sources have the potential to solve this conflicting problem, since the femtosecond pulse duration and the high photon flux density of XFELs allow the collection of diffraction data before samples are destroyed. So far, XFEL-CDI has visualized large viruses, biological cells and cell components such as chloroplasts and nuclei at resolutions of 30–100 nm.

However, the poor diffraction power of biological objects remains an obstacle to improving the resolution of electron density maps. Another serious problem in CXDI is the quality and incompleteness of experimental diffraction data. Iterative PR calculations starting from a diffraction pattern with poor signal-to-noise ratios and unobserved data (particularly in the area at lowest spatial frequency where there is a beamstop; Fig. 1) often diverge or yield an incorrect solution. A reliable initial phase is extremely helpful for overcoming these problems and can lead to the correct structure.

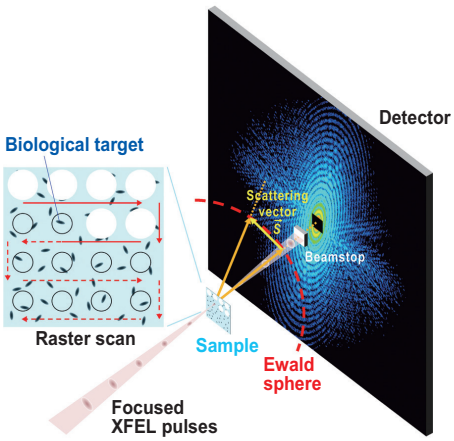

Fig. 1. Schematic illustration of XFEL-CDI experiments. In our scheme, biological targets are embedded in thin amorphous ice and raster-scanned with XFEL pulses. The direct beam transmitted through the sample is blocked by a beamstop, resulting in a lack of diffraction data at lower frequencies.

Recently, we have developed a new method to enhance diffraction signals from biological objects and to derive a reliable initial phase from their diffraction patterns alone [2]. Here, we introduce the concept behind this technique and demonstrate that the resolution is improved by a factor of two or more from a set of calculations based on our XFEL-CDI experiments at beamline **BL3** of SACLA [3,4].

We use colloidal gold (CG) particles and image the particles and biological targets together. Figure 2(a) shows a bacterial cell with four flagella and dispersed CG particles. The irradiation of an XFEL pulse on the whole sample yields an interference pattern between diffraction waves from both the biological target and the CG particles on the detector plane (Fig. 2(b)). Because the average electron density of gold is tenfold higher than that of biological objects, weak diffraction waves from the biological target are effectively enhanced to a detectable level by interference with strong waves from the CG particles. In fact, numerical calculations under the current experimental conditions at SACLA show that the diffraction pattern from the whole sample (Fig. 2(b)) extends to a more than twice wider range of spatial frequency than that of the diffraction pattern from the biological target alone (Fig. 2(c)). The diffraction pattern from the cell-CG model is dominated by the contribution from the CG particles, which display concentric ring patterns, and the interference term enhances the diffraction signals from the biological target by one order of magnitude, except for the valleys in the ring patterns (Fig. 2(d)).

The conventional PR from the diffraction pattern of the cell-CG model (Fig. 2(b)) does not converge to interpretable solutions mainly because of the lack of lower frequency information, which corresponds to the overall shape of the sample. In our scheme, the Patterson-search phasing method is adopted to derive the positions of the CG particles from the diffraction pattern, and the positions can be used in iterative PR calculations as an initial phase. Because of the large

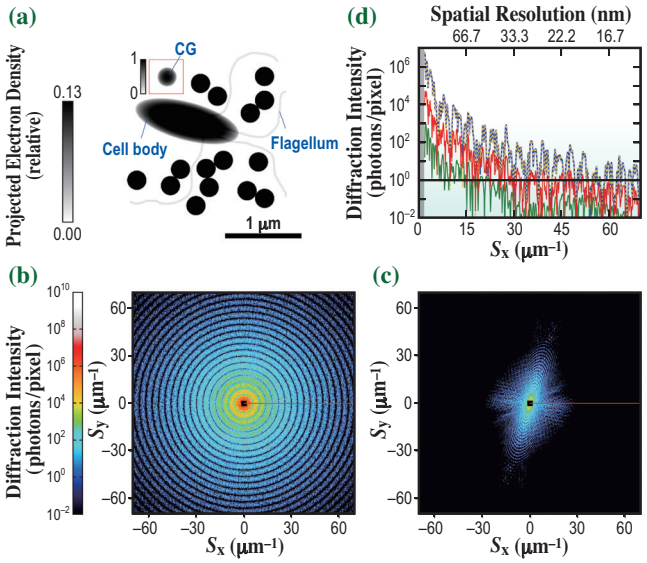

Fig. 2. **(a)** Sample for signal-enhanced XFEL-CDI. **(b)** Diffraction pattern calculated from the whole sample shown in (a). **(c)** Pattern obtained from the bacterial cell including the flagella in (a) alone. Poisson noises are added in (b) and (c). **(d)** Intensity profiles without noises along red horizontal lines in (b) and (c) calculated from the individual components: whole sample, blue solid line; bacterial cell, green solid line; CG particles, yellow dotted line; and magnitude of the interference term, red solid line. The missing region at the center is gray.

contribution from the CG particles (Fig. 2(d)), the initial phase approximates well that of the whole sample, and this leads to reliable reconstruction of the whole sample. This strategy is similar to the heavy atom method used for phasing in X-ray crystallography [5], but the CG particles are more powerful as the scattering from CG is much stronger.

In our calculations, the CG particles yielded clear peaks in a sharpened Patterson map (Fig. 3(a); see also Methods in [2]). Every peak represents the relative position (cross vector) between two gold particles. Then the absolute positions of the CG particles were determined by the Patterson superposition method [5] (Fig. 3(b)). By treating the positions of CG particles as a constraint, we reconstructed a projected electron density map of the CG particles through the PR calculation. Finally, we successfully obtained the map of the whole sample from the initial phase derived from the map of the CG particles (Fig. 3(c)). The reconstruction clearly reveals electron densities corresponding to the cell body and the four flagella, even though the projected electron density of a single flagellum is only 1.1% of that of the CG. In contrast, a map of the biological target reconstructed from the diffraction pattern of the cell alone is somewhat blurred, and the flagella are not correctly resolved (Fig. 3(d)). The spatial resolution of the map of the cell-CG model is estimated to be ~13 nm by Fourier ring correlation analysis, whereas the resolution of the cell-alone model is limited to ~29 nm. Thus, the method described here can improve the spatial resolution more than twofold under the current experimental setup.

As CG is a nonreactive material, this approach is compatible with imaging biological objects under physiological conditions. Flash-cooling of samples can maintain hydrated states and the integrity of cellular and subcellular structures. Thus, the combination of cryo-CXDI [3] and the signal enhancement with CG is well suited for imaging of biological structures. On the basis of the calculations reported here, cryo-XFEL-CDI with CG particles is presently under way, aimed at higher resolution and reliable structure analysis of complex biological targets [4].

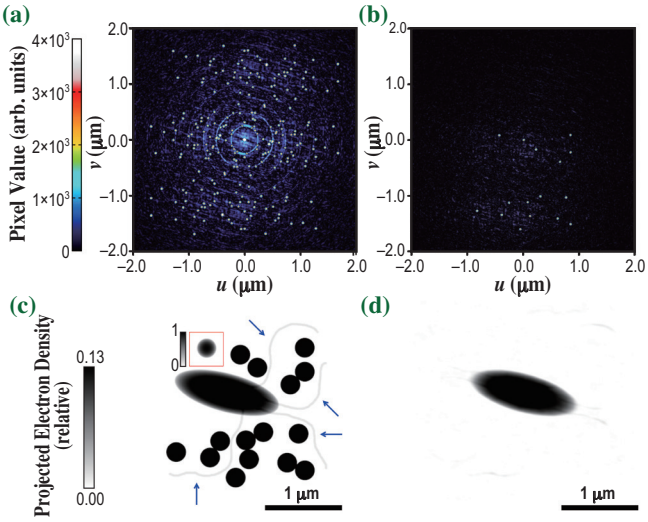

Fig. 3. **(a)** Sharpened Patterson map calculated from the diffraction pattern in Fig. 2(b). **(b)** Superposition minimum function map derived from panel (a) by Patterson search. Clear peaks are found at the positions of the CG particles. **(c)** Projected electron density map of the whole sample reconstructed from the pattern in Fig. 2(b) with the initial phases. **(d)** Map of the bacterial cell alone reconstructed from the pattern in Fig. 2(c).

Yuki Takayama and Koji Yonekura*

RIKEN SPring-8 Center

*E-mail: yone@spring8.or.jp

References

[1] J. Miao *et al.*: Science **348** (2015) 530.
[2] *Y. Takayama, S. Maki-Yonekura, T. Oroguchi, M. Nakasako and K. Yonekura: Sci. Rep.* ***5*** *(2015) 8074.*
[3] M. Nakasako *et al.*: Rev. Sci. Instrum. **84** (2013) 093705.
[4] Y. Takayama and K. Yonekura: Acta Crystallogr. A **72** (2016) 179.
[5] G.M. Sheldrick: Methods in Enzymol. **276** (1997) 628.